Basics of ocean color remote sensing

Getting information about in-water constituents from the color of the oceans.

Major issues:

- Atmospheric correction
- Avoidance of sun glint
- White cap correction
- Calibration
- Inversion of Lw/Ed to obtain IOP.

Ocean Color Remote Sensing to Chlorophyll

$E_{PAR}(0)$

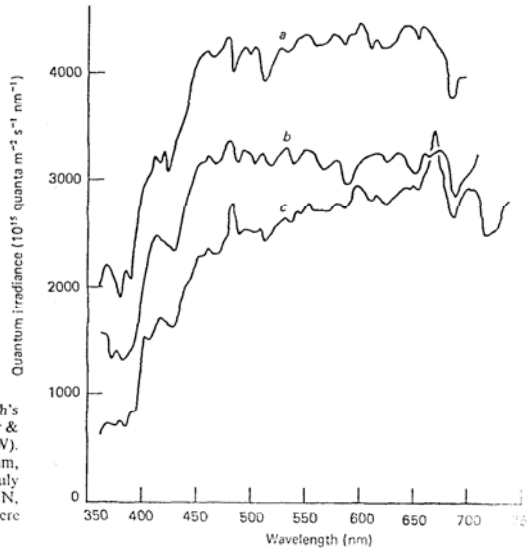

2.3. Spectral distribution of solar quantum irradiance at the Earth's surface at three geographical locations (plotted from the data of Tyler & Smith, 1970). (*a*) Crater Lake, Oregon, USA (42°56′ N, 122°07′ W). Elevation 1882 m. 1100–1125 h, 5th August 1966. (*b*) Gulf Stream, Bahamas, Atlantic Ocean (25°45′ N, 79°30′ W). 1207–1223 h, 3rd July 1967. (*c*) San Vicente reservoir, San Diego, California, USA (32°58′ N, 116°55′ W). 0937–0958 h, 20th January 1967. All the measurements were made under clear skies.

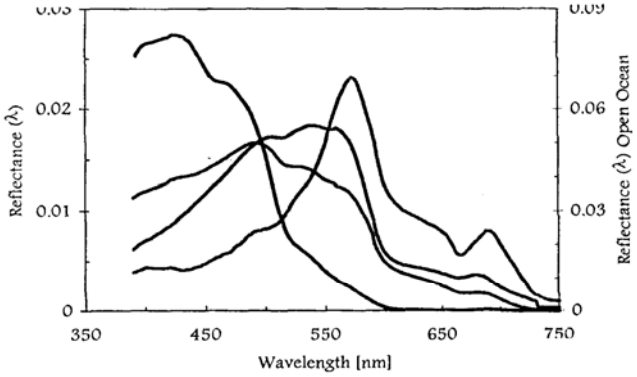

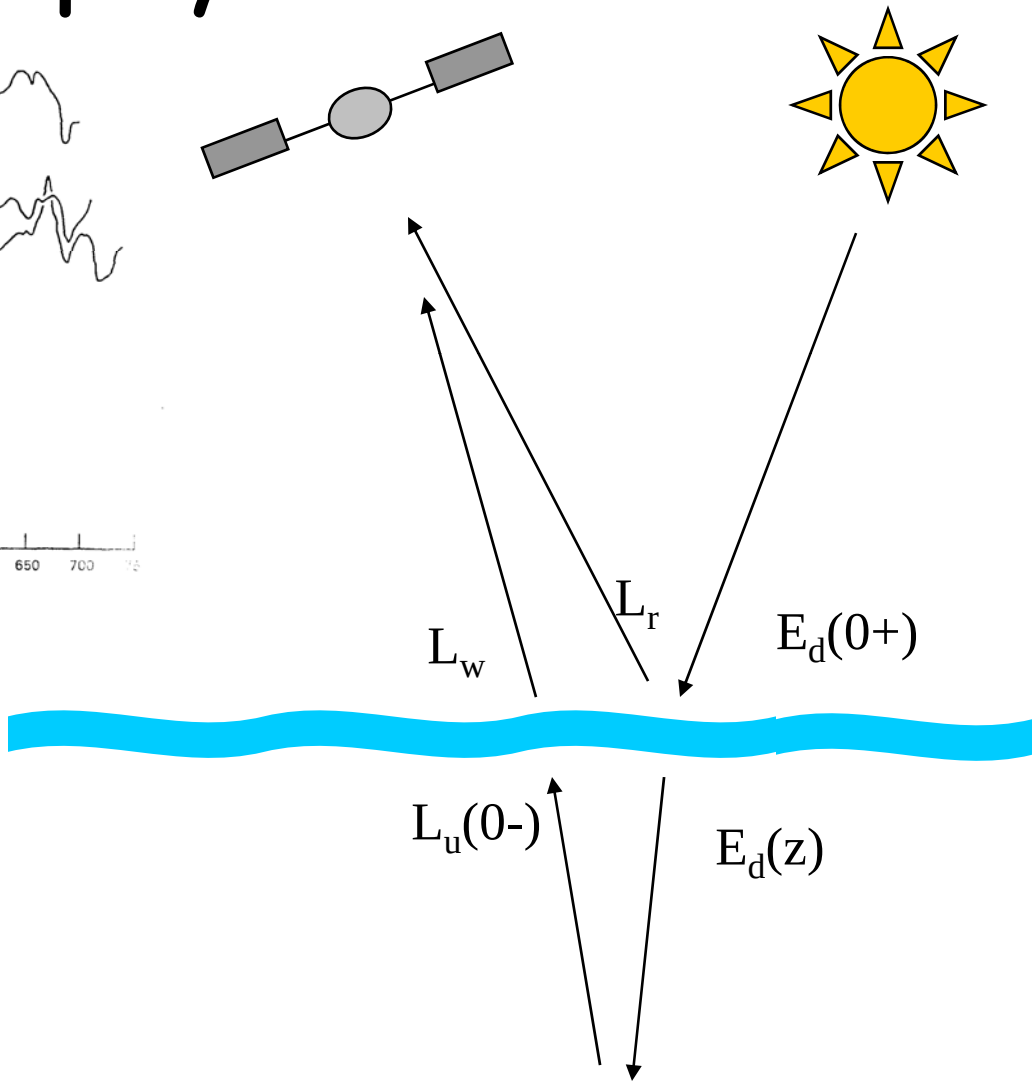

2 steps to help with the interface

Transmission across the air–water interface

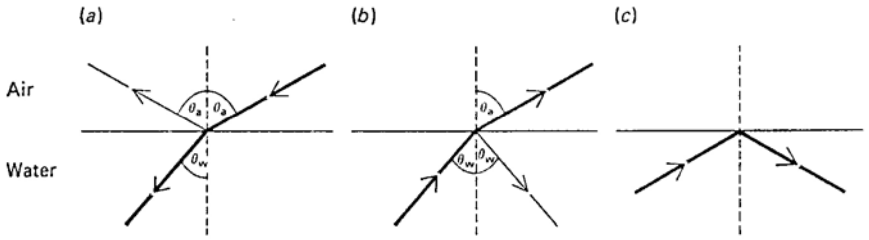

Fig. 2.11. Refraction and reflection of light at air–water boundary. (*a*) A light beam incident from above is refracted downwards within the water: a small part of the beam is reflected upwards at the surface. (*b*) A light beam incident from below at a nadir angle of 40° is refracted away from the vertical as it passes through into the air: a small part of the beam is reflected downwards again at the water–air boundary. (*c*) A light beam incident from below at a nadir angle greater than 49° undergoes complete internal reflection at the water–air boundary.

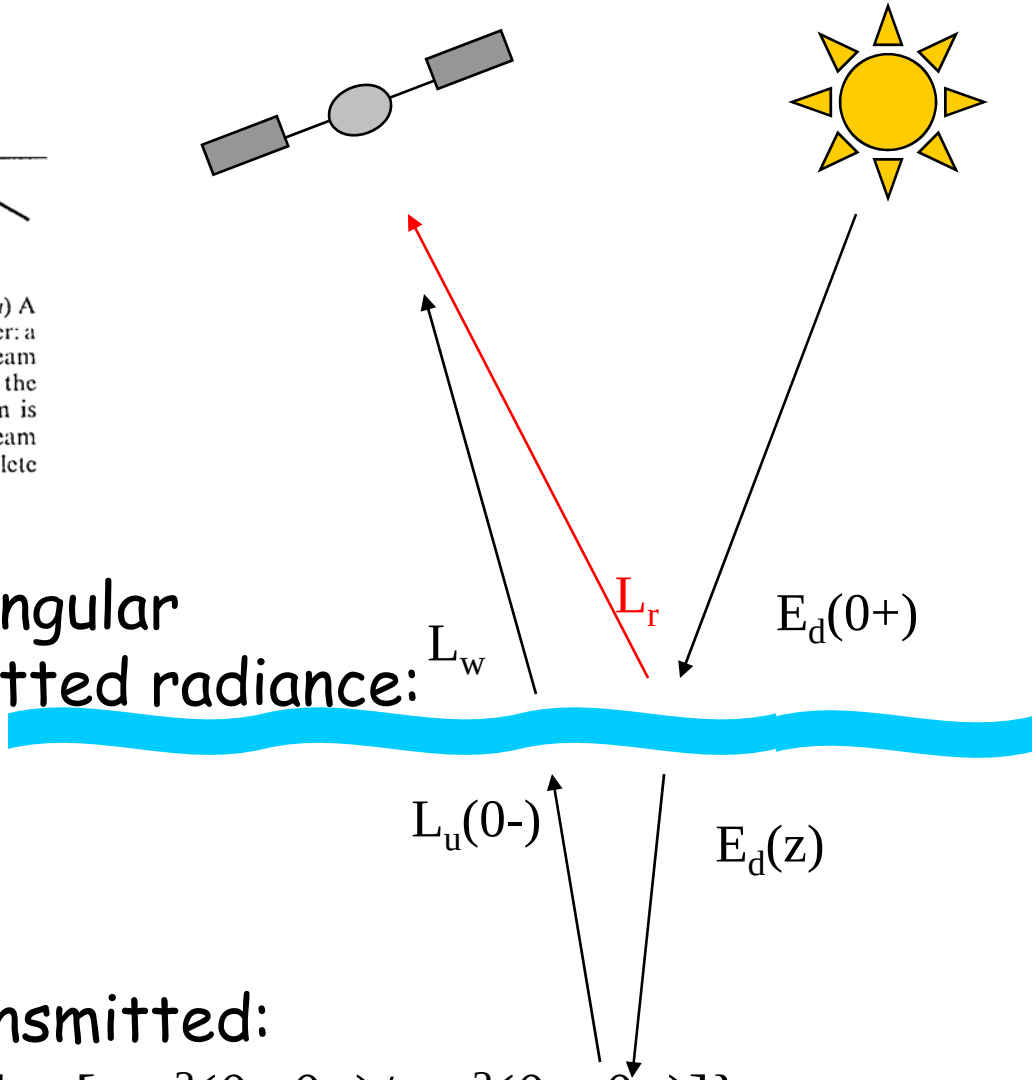

Snell's Law describes the angular distribution of the transmitted radiance:

$\sin\theta_a/\sin\theta_w = n_w/n_{air} \sim 1.34$

Fresnel defines amount transmitted:

$$r = 0.5\{[\sin^2(\theta_a-\theta_w)/\sin^2(\theta_a+\theta_w)] + [\tan^2(\theta_a-\theta_w)/\tan^2(\theta_a+\theta_w)]\}$$

Ocean Color Remote Sensing to Chlorophyll

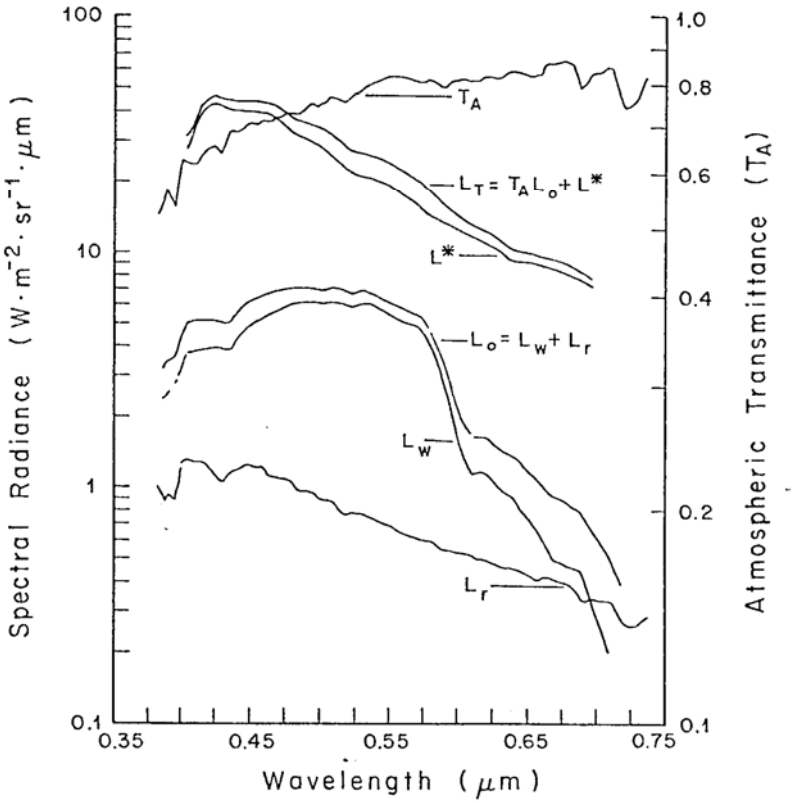

Figure 7.14 Computed spectral radiances that contribute to the light seen by a satellite instrument viewing typical sunlit seas. Note that the upwelling radiance from the sea, L_w, is much smaller than the light reflected and scattered by the atmosphere, L^*. Also shown is the vertical transmittance T_A of the atmosphere (from Wilson and Austin, 1978).

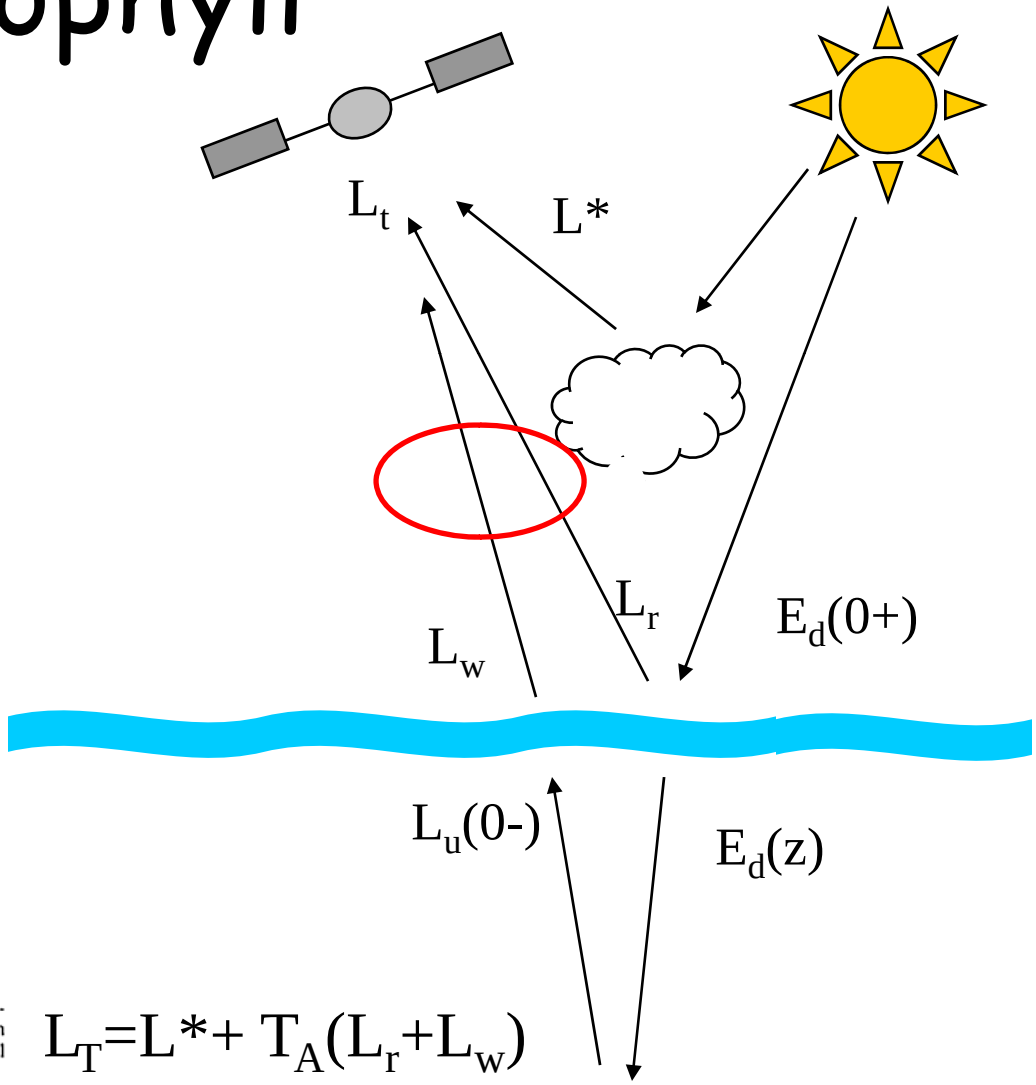

$$L_T = L^* + T_A(L_r + L_w)$$

Ocean Color Remote Sensing to Chlorophyll

CZCS

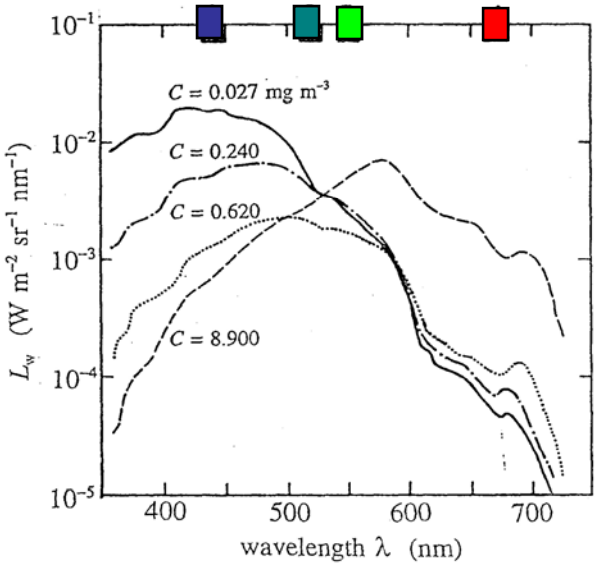

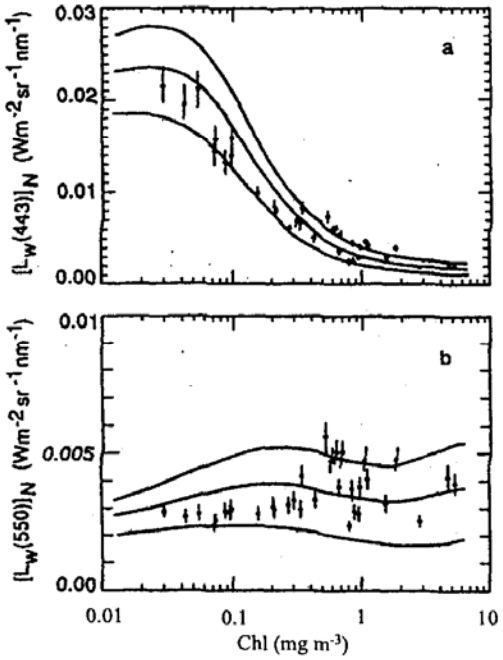

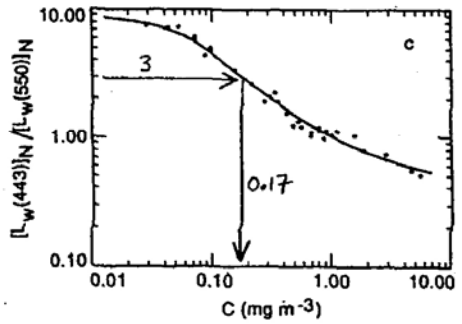

Figure 22. In panels (a) and (b), the solid lines are values of the normalized water-leaving radiances $[L_w(\lambda)]_N$ at λ = 443 and 550 nm, respectively, as *predicted by various models that relate* $[L_w(\lambda)]_N$ *to the* chlorophyll concentration *C*. The dots are measured values of $[L_w(\lambda)]_N$. Panel (c) shows the predicted (line) and observed *ratio* of the $[L_w(\lambda)]_N$ values of panels (a) and (b). (redrawn from Gordon, *et al.*,[78] with permission)

Variations in the radiance ratios were interpreted solely as a response to variations in Chlorophyll concentration

Coastal Zone Color Scanner

Atmospheric Correction

- Gordon and Clark 1981 CZCS
- Gordon and Wang 1998 SeaWiFS
- Gordon and others 2002 MODIS

Water-leaving radiance

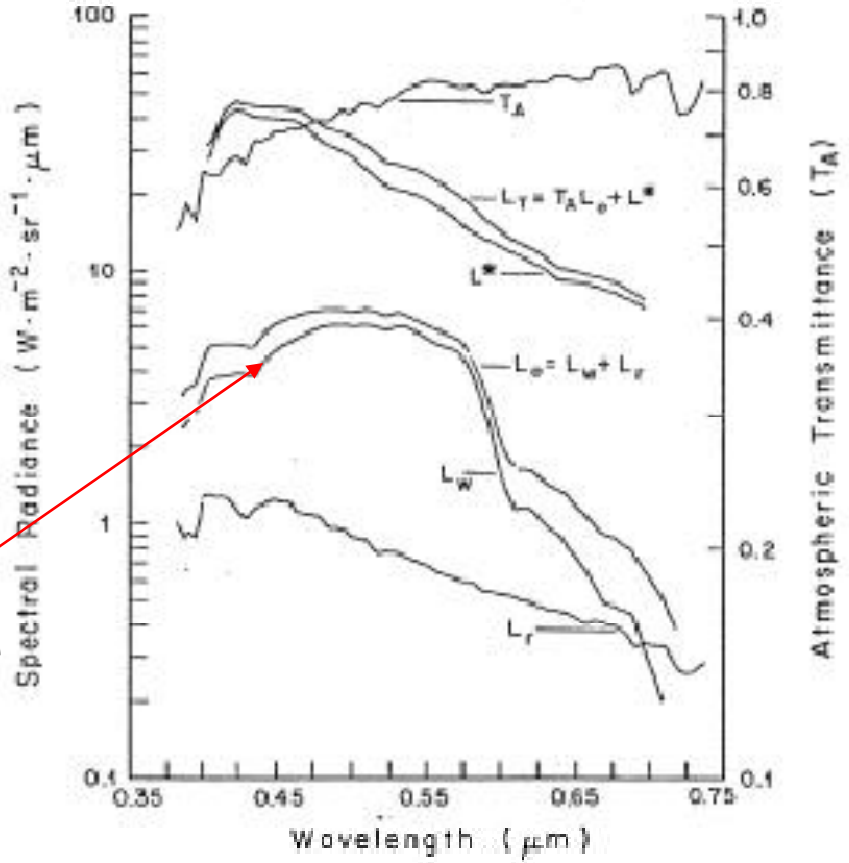

After atmospheric correction…$L_w(\lambda)$

Variations in the radiance ratios were interpreted solely as a response to variations in Chlorophyll concentration

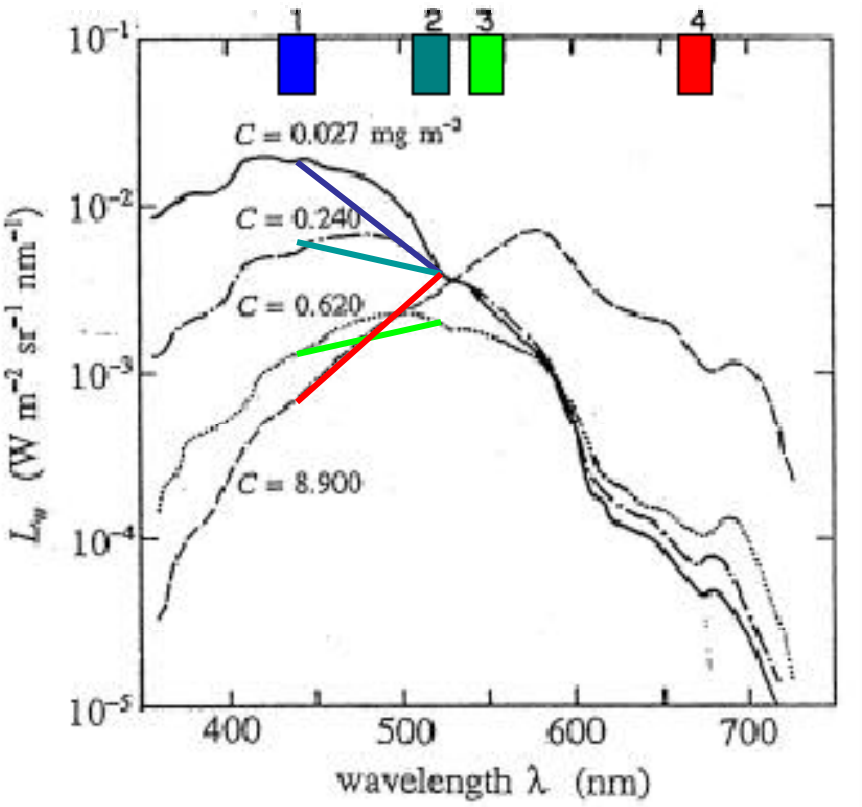

And the relationship between radiance ratios and pigment concentration…

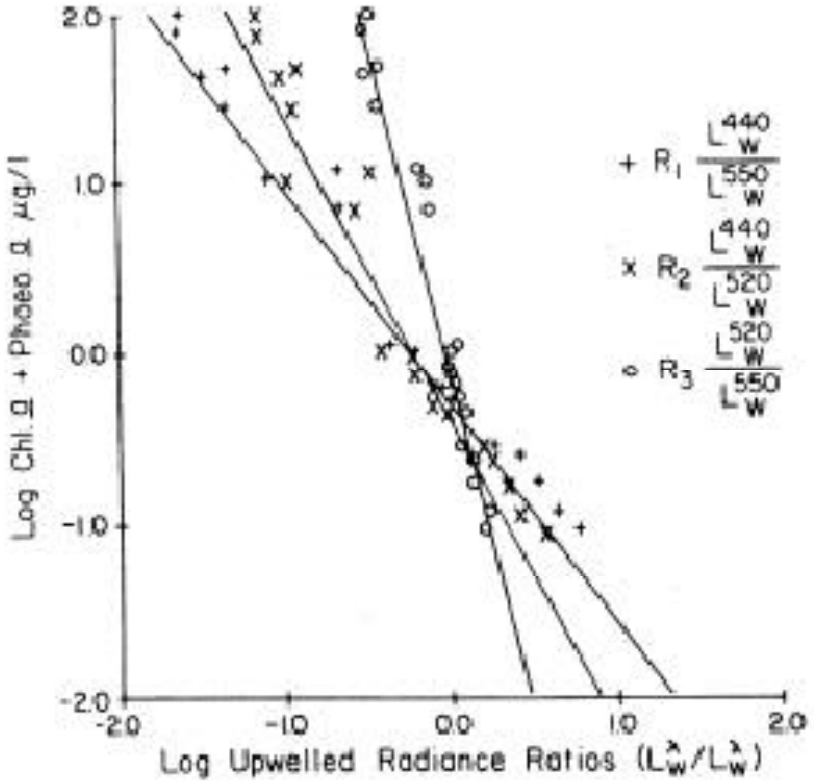

Figure 7.12 Ratios R of upwelling radiance just above the sea surface between pairs of light bands, as a function of the chlorophyll and phaeopigment concentration at the surface. The superscript on L refers to the wavelength in nanometers (from Gordon and Clark, 1980).

But variations in ocean color are due to more than just chlorophyll

Approximations to the RTE
Successive order scattering method
Monte Carlo simulations
(Gordon, Zaneveld, Kirk, Morel…)

All lead to:

$R \sim b_b/(a+b_b)$

Which indicates that variations in R can be explained by variations in absorption and backscattering.

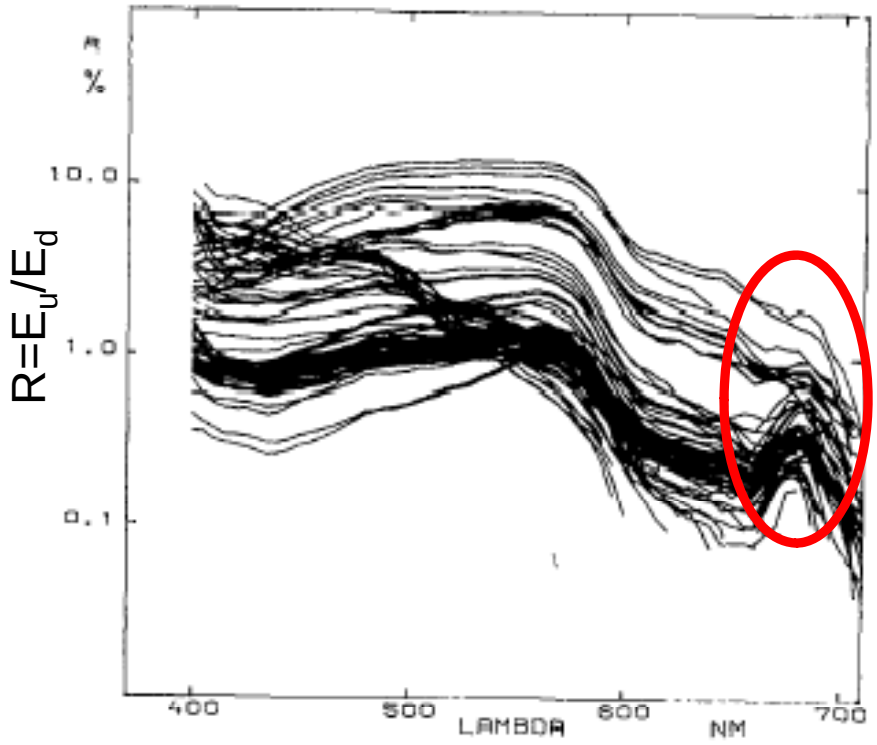

Fig. 1. Reflectance ratio $R(\lambda)$, expressed in percent, plotted with logarithmic scale vs. wavelength λ in nm, for 81 experiments in various waters. Same units and scales also used in Figs. 4, 5, 6, 7, and 11.

Morel and Prieur, 1977. Analysis of variations In ocean color. L&O, 22:709-722.

Spectral backscattering parameterization

$b_b(\lambda) = b_{bw}(\lambda) + b_{bp}(\lambda)$

$b_b(\lambda) = b_{bw}(\lambda_o)\,\Lambda^{nw} + b_{bp}(\lambda_o)\,\Lambda^{np}$

Where $\Lambda = \lambda/\lambda_o$

$b_b(\lambda) = b_b(\lambda)\eta'_o\Lambda^{nw} + (1-\eta'_o)\Lambda^{np}$

Where $\eta'_o = b_{bw}/b_b$

n_w and n_p describe the spectral slope of b_{bw} and b_{bp}, respectively.
n_w = -4.3 while n_p ranges from 0 to -1

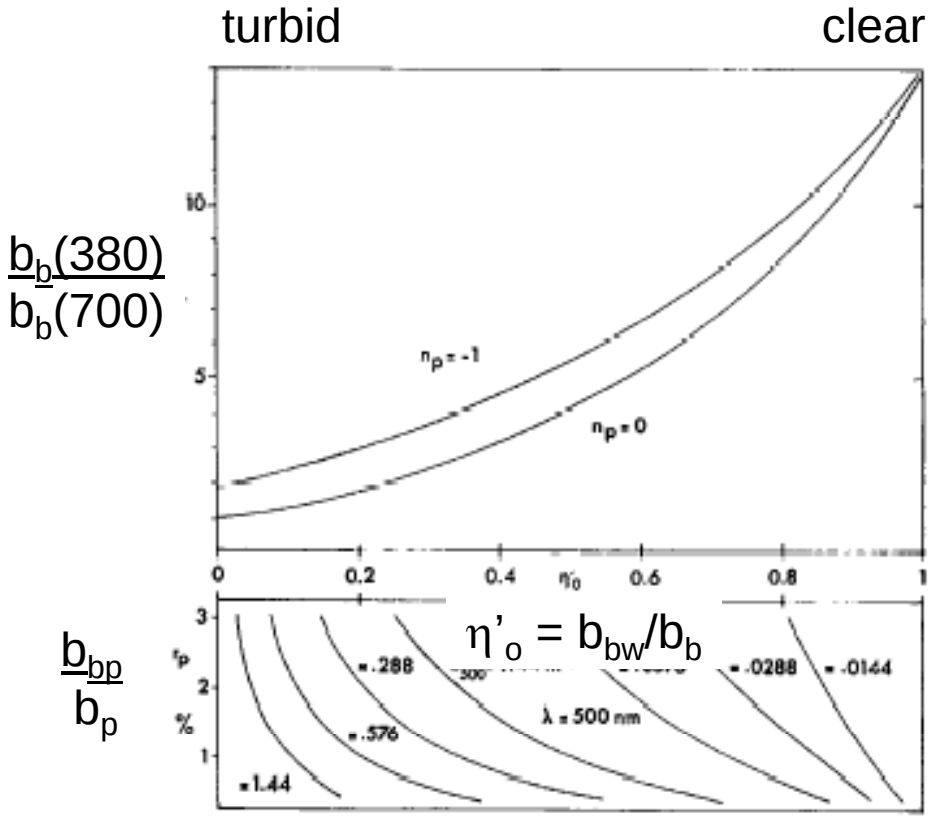

Fig. 2. Upper—ratio of back-scattering at $\lambda = 380$ and 700 nm plotted vs. parameter η'_o. Lower—variations of η'_o with parameter r_p for selected values of b, scattering coefficient at $\lambda = 500$ nm (in m^{-1}).

Case I: Blue Water

- $R = (b_{bw} + b_{bp})/a_w$

Where b_w was modeled using Rayleigh theory, c_w was measured and b_{bw} and a_w were computed

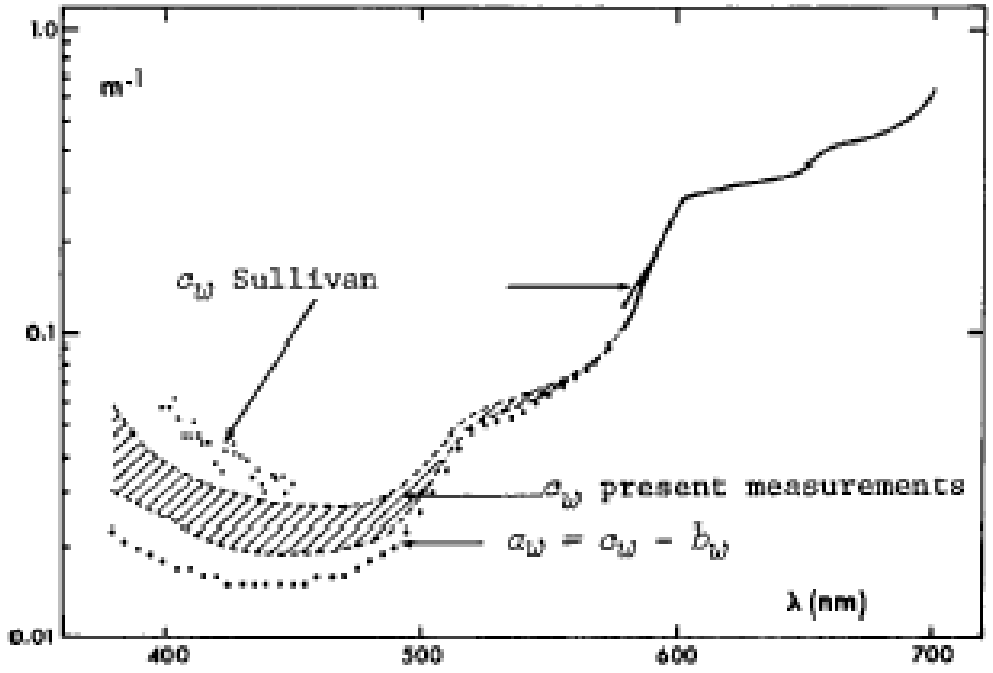

Fig. 3. Attenuation, $c_w(\lambda)$, and absorption coefficient, $a_w(\lambda)$, expressed in m^{-1}, for pure water.

Case I: Blue Water

- $R = (b_{bw} + b_{bp})/a_w$

Where b_w was modeled using Rayleigh theory, c_w was measured and b_{bw} and a_w were computed

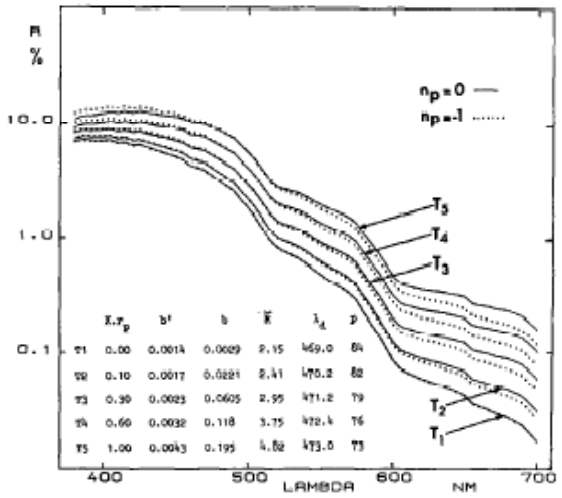

By varying b_{bp} and n_p, a range of clear water reflectance spectra were generated

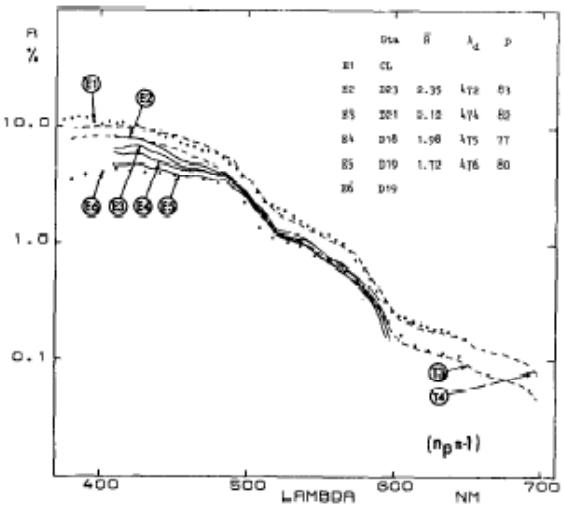

And compared to clear water observations In Crater Lake and the Sargasso Sea

Case I: V-type Green Water

"…chlorophyll concentration is high relative to the scattering coefficient"

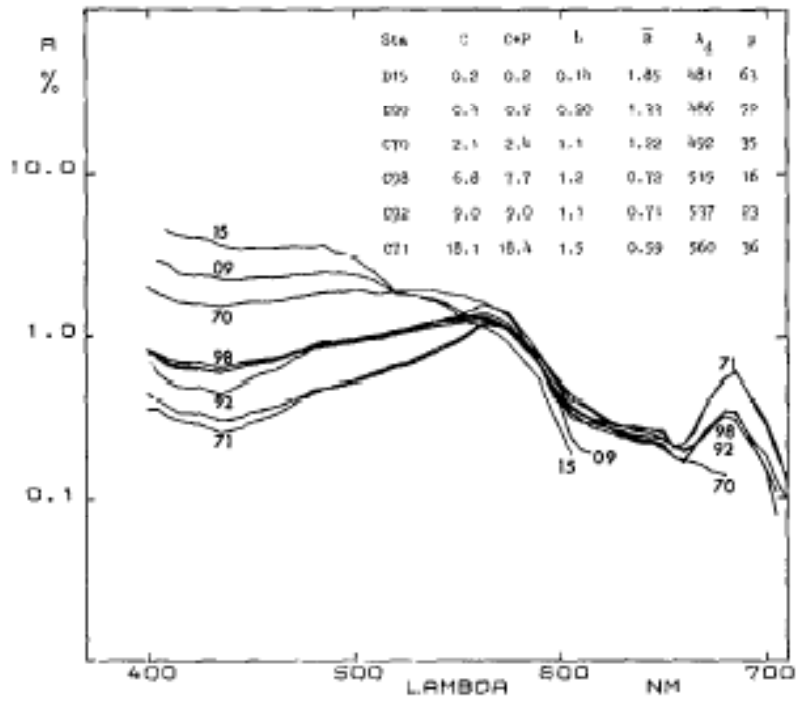

Fig. 6. Experimental $R(\lambda)$ curves for different stations listed in inset: D stations—Discoverer cruise; C stations—CINECA 5-Charcot cruise. C and C+P—chlorophyll *a* and the chlorophyll *a* + phcophytin *a* concentration in mg m^{-3}; *b*—scattering coefficient at 550 nm. Curves illustrate case 1 (*see text*).

Case II: U-type Green Water

"…waters relatively higher in inorganic particles than in phytoplankton"

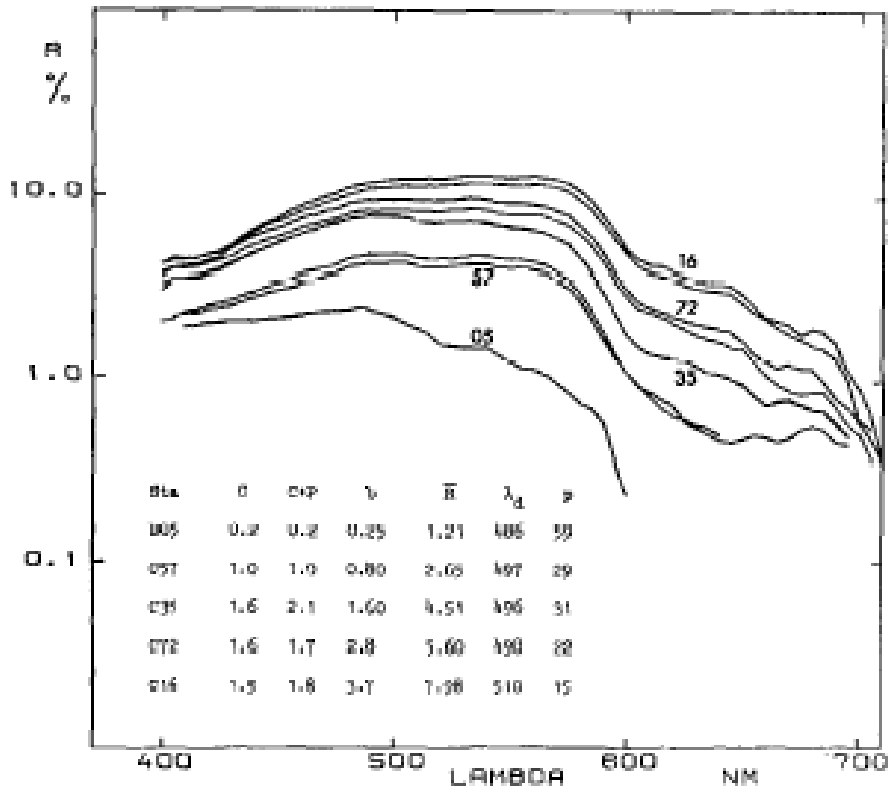

Fig. 7. Experimental $R(\lambda)$ curves illustrating case 2 (*see text*). Symbols same as for Fig. 6.

The model

$R \sim b_b/a$

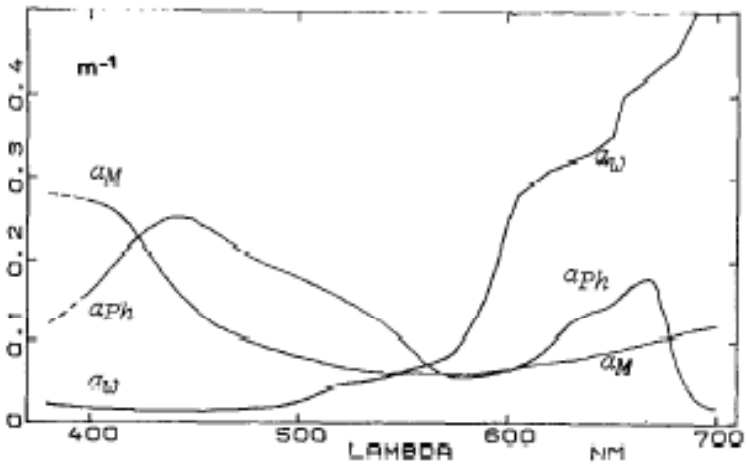

Fig. 10. Spectral values, expressed in m^{-1}, of absorption coefficients: a_w—for pure water; a_{PA}—for natural phytoplankton pigments at concentration corresponding to Chl *a* concentration of 10 mg m^{-3}; a_M—for suspended and dissolved materials, apart from algae, at concentration corresponding to scattering coefficient of 2 m^{-1} (at 550 nm).

$$a = a_w + [Chl+Pheo]a^*_\phi + b\, a^*_m$$

$b_b = b_{bw} + (b-b_w)(b_{bp}/b_p)$

(know, b_w,b_{bw} measure b

Let b_{bp}/b_p be constant)

The results

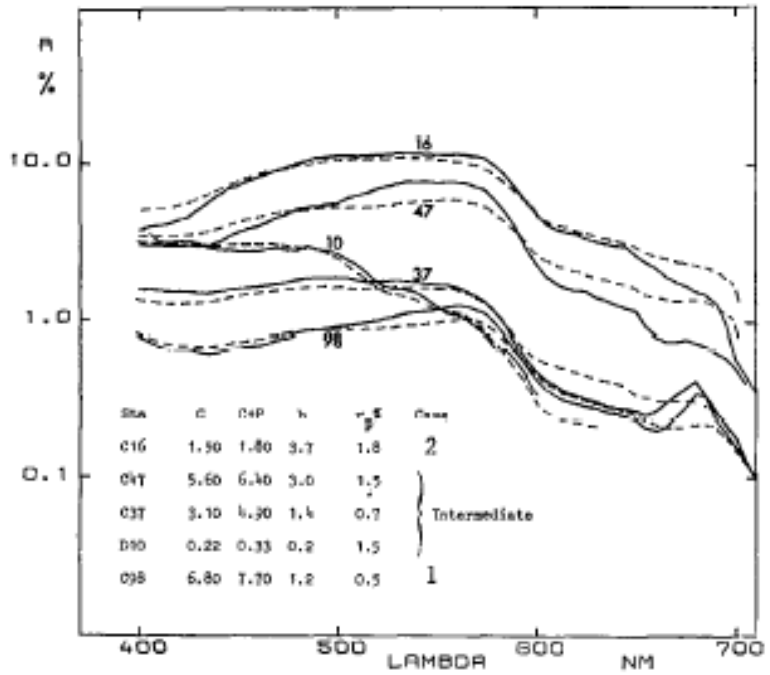

Fig. 11. Solid curves—experimental $R(\lambda)$ curves for stations listed in inset (D for Discoverer, C for Charcot cruises). Dashed curves—theoretical $R(\lambda)$ curves (same stations) computed with measured scattering coefficient b (at 550 nm, in m^{-1}) and pigment concentration (chlorophyll a + pheophytin a, column C+P, in mg m^{-3}). Column r_p gives adjusted values of this parameter to obtain best agreement in each case between computed and actual $R(\lambda)$ curves.

Force the model to fit the observations at 500 nm, the rest of the spectrum fits very well.

The results

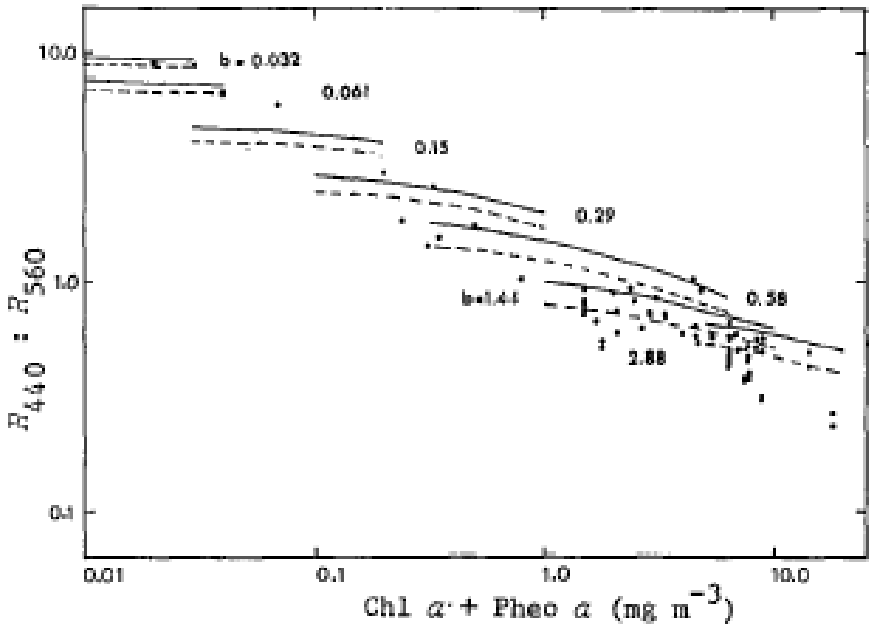

Fig. 12. Ratio of reflectance ratios at 440 and 560 nm, plotted vs. pigment concentration (Chl a + Pheo a, in mg m^{-3}). Both scales logarithmic. Dots—experimental values; curves—computed variations of same ratio ($n_p = -1$: solid lines; $n_p = 0$: dashed lines).

An order of magnitude variation in Pigment for given reflectance ratio.

Due to combined spectral variations in absorption and backscattering.

Variations in ocean color are due to more than simply variations in Chl

1980's Invert R to retrieve Chl

$R = Q\, b_b/(a+b_b)$

$a = fcn\,(w, Chl, ys)$

$b_b = b_{bw} + A*Chl^B$

Modeled Lu as a function of Chl and solved for unknowns

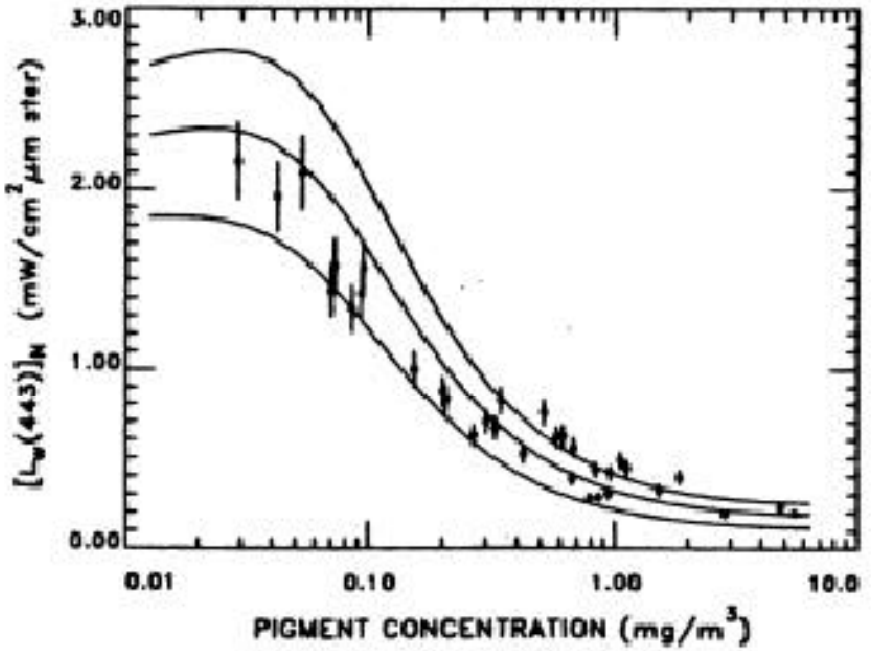

Fig. 1. Value of $[L_w(443)]_N$ as a function of the pigment concentration. The curves are the results of the model with the upper curve corresponding to $b^0 = 0.45$ m^{-1}, the middle curve to $b^0 = 0.30$ m^{-1}, and the lower curve to $b^0 = 0.12$ m^{-1}. The points are *Clark's* [1981] experimental measurements.

Gordon et al. 1988

But you can do better with ratios

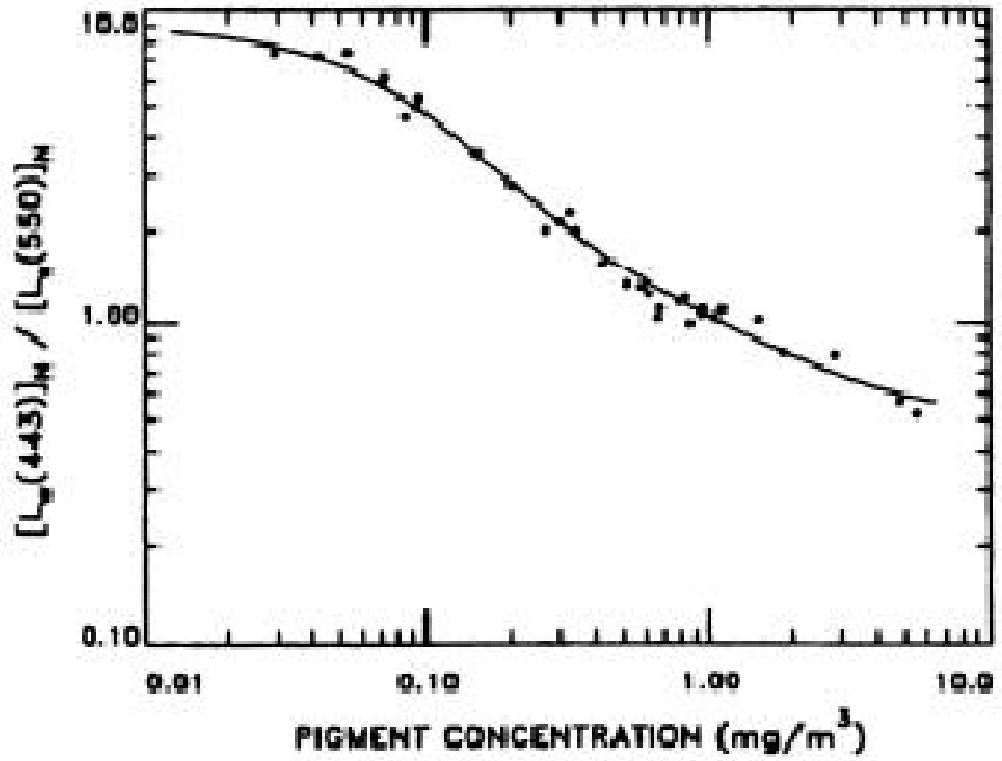

Fig. 6. The radiance ratio $[L_w(443)]_N/[L_w(550)]_N$ as a function of the pigment concentration. The curve is the result of the model, with $b^\circ = 0.20\ m^{-1}$. The points are *Clark's* [1981] experimental measurements.

1990's invert R to obtain IOPs

Definition $R = Eu/Ed$ or Lu/Ed

Theory $R = F_q\, b_b/(a+b_b)$

By linear superposition

$a = \Sigma_i\, C_i\, a^*_i(\lambda)$ and $b_b = \Sigma_j\, C_j\, b_{bj}^*(\lambda)$

So set measurement = theory

$R = \Sigma_j\, C_j\, b_{bj}^*(\lambda) / [\Sigma_i\, C_i\, a^*_i(\lambda) + \Sigma_j\, C_j\, b_{bj}^*(\lambda)]$

Define the backscattering and absorption spectra, solve for C's

Definitions of a, b_b spectra parameterizations

- Lee et al. 1994
  - $b_{bp}/b = X[400/\lambda]^Y$
  - a_ϕ polynomial expansion of Chl
  - a_{CDOM} exponential function
- Roesler and Perry 1995
  - $b_{bp} = b_{bp}(\lambda_o)\,\lambda^0 + b_{bp}(\lambda_o)\,\lambda^{-1}$
  - a_ϕ dimensionless spectrum
  - $a_{CDOM+nap}$ exponential function
- Garver and Siegel 1997
  - $b_{bp}(\lambda o)\,\lambda^{-n}$
  - $a_\phi = a^*_\phi$ Chl
  - a_{nap} exponential function

Solution Techniques

- Linearization and regression
  - Hoge and Lyon 1996, 1999
  - Wang et al., 2005
- Non-linear least squares regression
  - Lee et al. 1994
  - Roesler and Perry 1995
  - Garver and Siegel 1997
- Modified non-linear regression
  - Maritorena et al. 2002

Lee, Z., Carder, K. L., Hawes, S. K., Steward, R. G., Peacock, T. G., & Davis, C. O. (1994). A model for interpretation of hyperspectral remote-sensing reflectance. *Applied Optics, 33*.

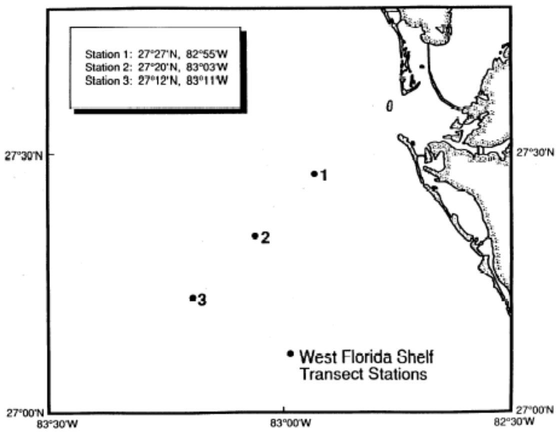

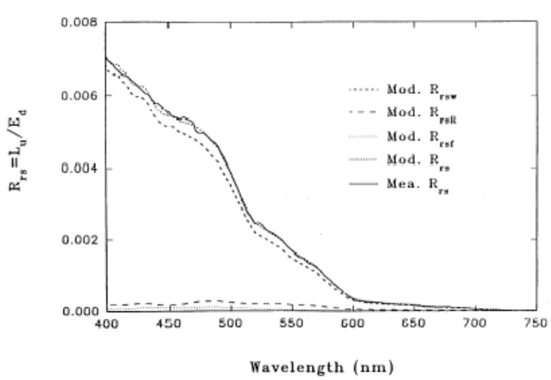

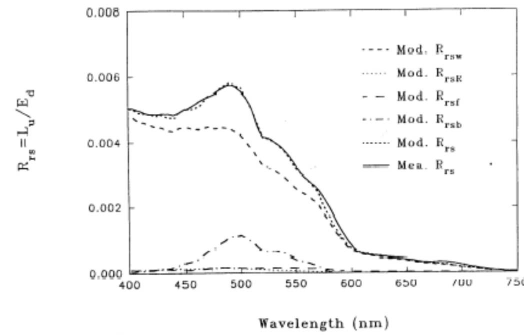

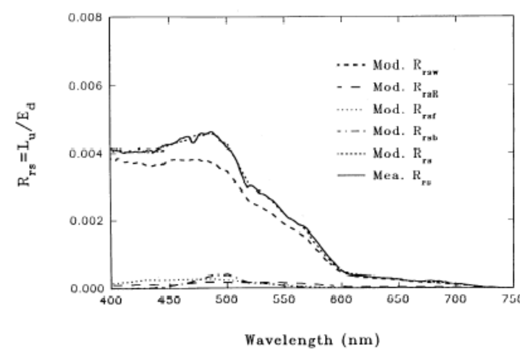

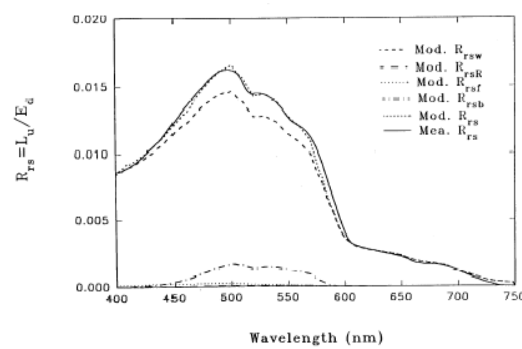

Hoge, F. E., Wright, C. W., Lyon, P. E., Swift, R. N., & Yungel, J. K. (1999). Satellite retrieval of inherent optical properties by inversion of an oceanic radiance model: A preliminary algorithm. *Applied Optics, 38*(3), 495-504.

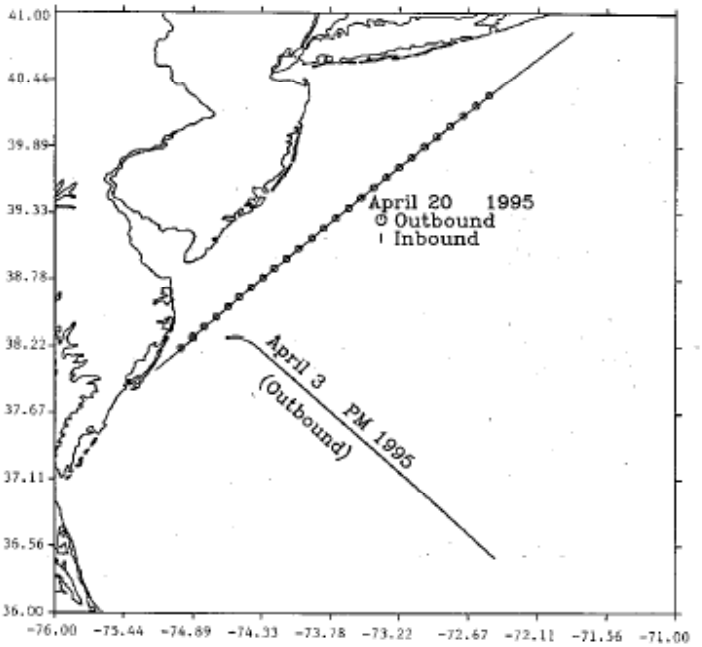

Fig. 1. Flight location of the AOL system and spectroradiometers aboard the NASA P-3B aircraft during the afternoon of 3 April 1995 is shown by the outbound southeast ground track line. This flight traversed five water masses: coastal, shelf, slope, Gulf Stream, and Sargasso Sea. Flight of the AOL system and spectroradiometers aboard the NASA P-3B aircraft on 20 April 1995 is shown by the outbound (toward the northeast) and inbound (toward the southwest) ground track lines. These latter track lines traversed only shelf and coastal water types.

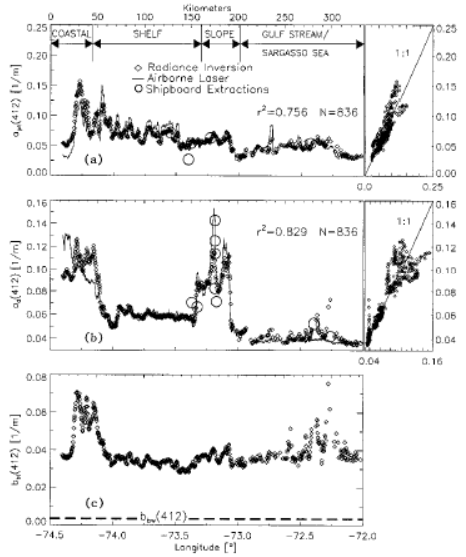

Fig. 2. (a) Along-track profile of phytoplankton absorption coefficient at 412 nm, $a_{ph}(412)$, retrieved from airborne water-leaving radiances plotted with chlorophyll absorption derived from concurrent airborne laser-induced F/R measurements obtained on the outbound portion of a flight to the Sargasso Sea during the afternoon of 3 April 1995. These parameters are also graphed as a scatterplot immediately to the right of the profile presentation. Limited absorption values derived from the supporting ship chlorophyll measurements are shown plotted as open circles. (b) Along-track profile of the CDOM and detritus absorption coefficient at 412 nm, $a_d(412)$, retrieved from the airborne water-leaving radiances plotted along with CDOM absorption measurements derived from airborne laser-induced CDOM F/R. These parameters are also graphed in the form of a scatterplot immediately to the right of the profile presentation. A limited number of supporting ship-derived CDOM absorption measurements are shown as open circles. (c) Along-track profile of the TCB coefficient, $b_{bl}(412)$, retrieved from the airborne water-leaving radiances. No truth data were available to validate the retrieved TCB.

Hoge, F. E., & Lyon, P. E. (1996). Satellite retrieval of inherent optical properties by linear matrix inversion of oceanic radiance models: An analysis of model and radiance measurement errors. *Journal of Geophysical Research-Oceans, 101*(C7), 16631- 16648

Optimization of a semianalytical ocean color model for global-scale applications

Stéphane Maritorena, David A. Siegel, and Alan R. Peterson

20 May 2002 / Vol. 41, No. 15 / APPLIED OPTICS 2705

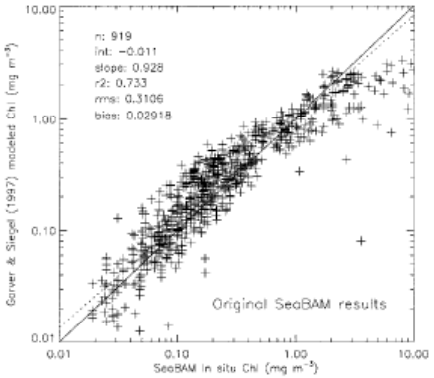

Fig. 1. Chl retrievals of the Garver–Siegel model[5] with its initial set of parameters and the SeaBAM[4] data.

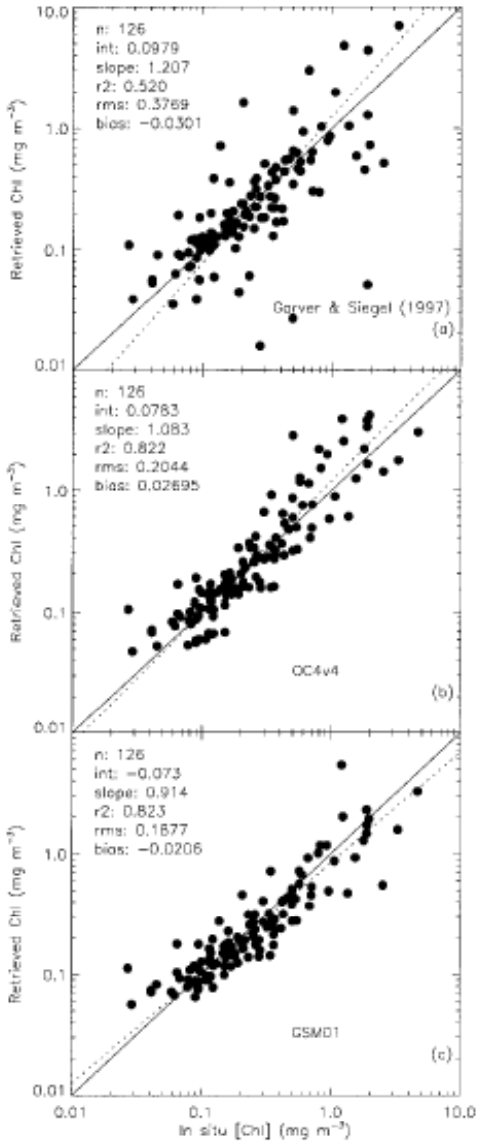

Fig. 5. Chl retrievals generated by the optimized model with tl *in situ* $L_{wN}(\lambda)$ data from the SeaWIFS match-up data set versus *situ* Chl data from that same data set: (a) the original Garver ar Siegel model,[5] (b) OC4v4, and (c) the GSM01 model.

2000's: Getting more than a and b_b from R inversions

Reports of the International
Ocean-Colour Coordinating Group

An Affiliated Program of the Scientific Committee on Oceanic Research (SCOR)
An Associate Member of the Committee on Earth Observation Satellites (CEOS)

IOCCG Report Number 5, 2006

Remote Sensing of Inherent Optical Properties: Fundamentals, Tests of Algorithms, and Application

Editor:
ZhongPing Lee (Naval Research Laboratory, Stennis Space Center, USA)

Report of an IOCCG working group on ocean-colour algorithms, chaired by ZhongPing Lee and based on contributions from (in alphabetical order):

Robert Arnone, Marcel Babin, Andrew H. Barnard, Emmanuel Boss,
Jennifer P. Cannizzaro, Kendall L. Carder, F. Robert Chen, Emmanuel Devred,
Roland Doerffer, KePing Du, Frank Hoge, Oleg V. Kopelevich,
ZhongPing Lee, Hubert Loisel, Paul E. Lyon, Stéphane Maritorena,
Trevor Platt, Antoine Poteau, Collin Roesler, Shubha Sathyendranath,
Helmut Schiller, Dave Siegel, Akihiko Tanaka, J. Ronald V. Zaneveld

Obtaining depth and bottom types from hyper-spectral Rrs:

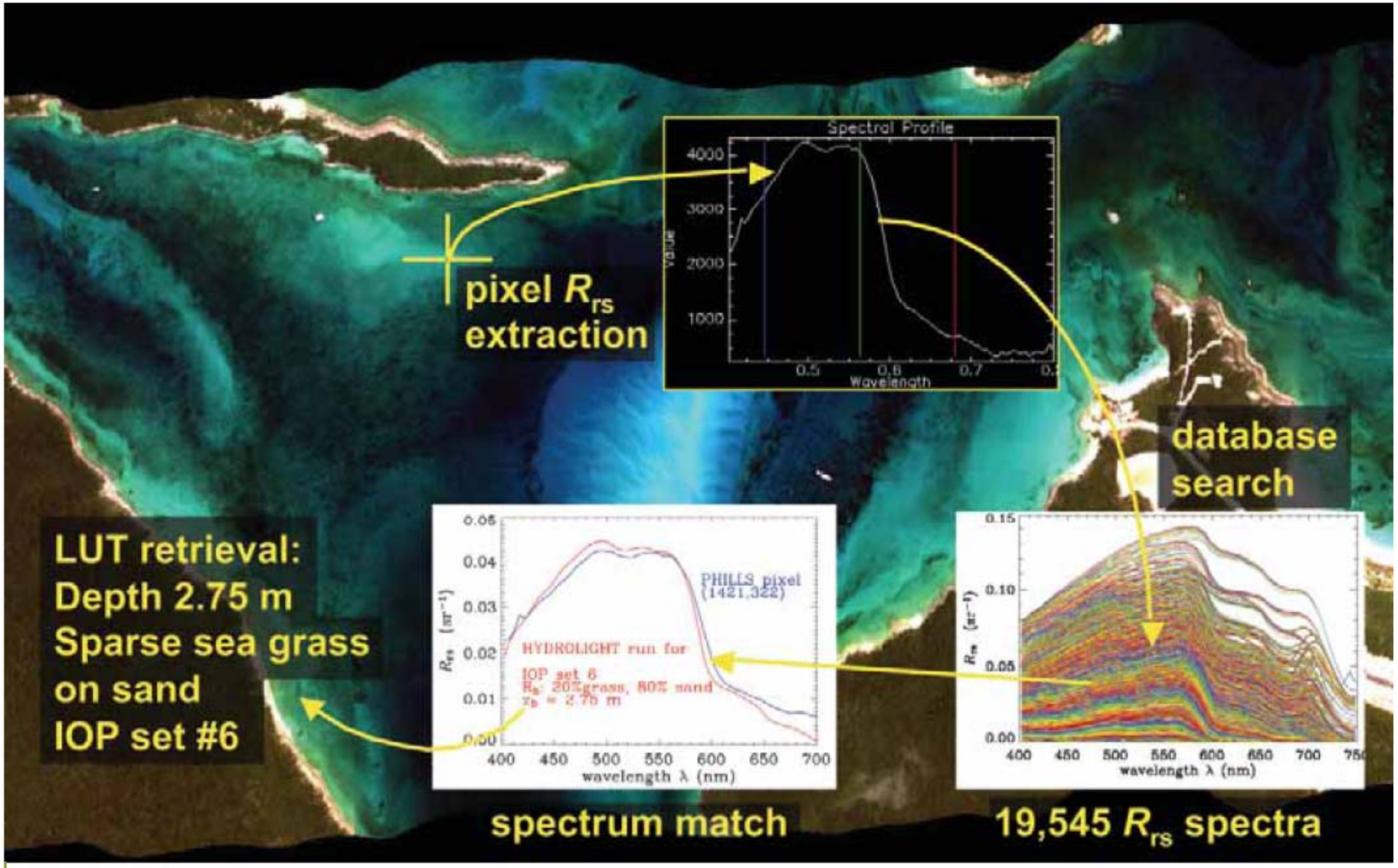

Figure 3. An image of Adderly Cut, Lee Stocking Island, Bahamas from the PHILLS hyperspectral scanner. Each pixel in the image represents the spectral remote sensing reflectance (R_{rs}) at that point. The observed spectrum is then compared to a look-up table (LUT), a database of spectra compiled for a wide range of depths, bottom types, and water types. The depth and bottom type of the best-fit modeled spectrum is then associated with the image pixel.

Mobley et al.

Detection of phytoplankton species from the Physat method

nLw_{obs} and Chl-a
from remote sensing or in-situ

↓

Selection criteria
(open ocean waters, τ_a<0.15)_

↓

$nLw^* = nLw_{obs} / nLw_{ref}$(Chl-a)_

↓

Dominant group for the pixel
if nLw* is in one 'of the predefined
envelop established from in situ
species identification and coincident
SeaWiFS nLw spectra '

Example : Dominant species for January 2001.
Most frequent dominant group for a month
on a 1x1 degree grid

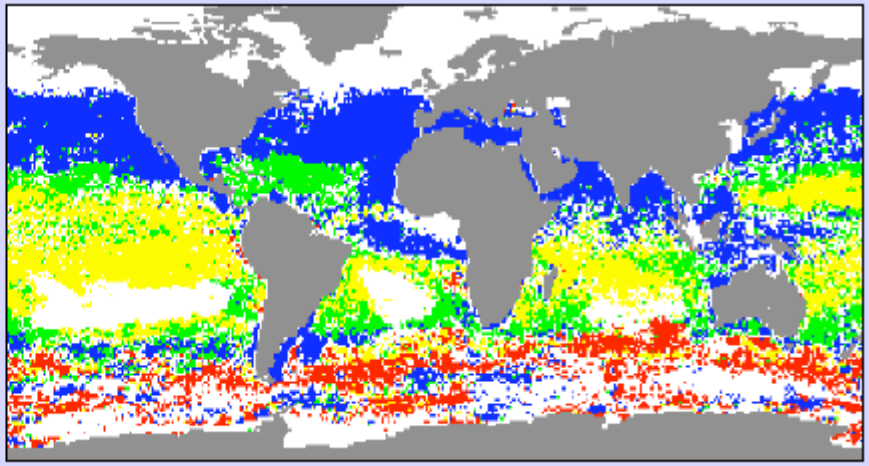

SLC (Synechococcus Like Cyanobacteria)

Alvain et al., 2005

Loisel et al., 2006: spectral slope of backscattering (potential information on size)

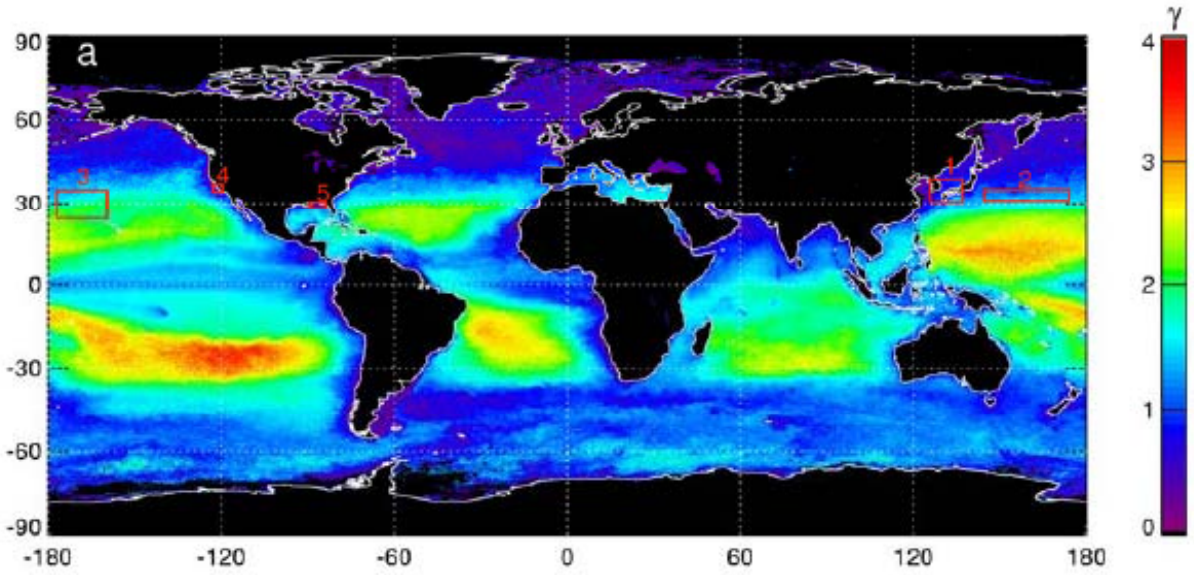

$b_{bw} \sim \lambda^{-4.3}$

$b_{bp} \sim \lambda^{0}$

$b_{bp} \sim \lambda^{-1}$

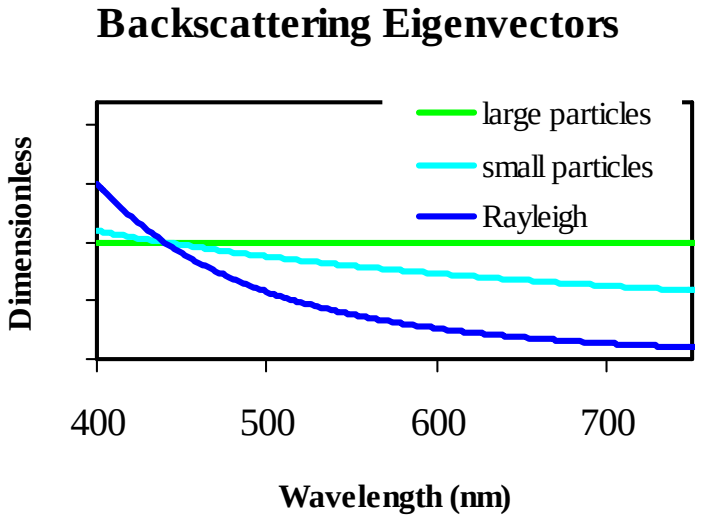

An alternative approach to NPP:

[chl]/C_{phyto} is directly related to phytoplankton growth rate.

If we know the growth irradiance, and [chl]/C_{phyto} we can predict how fast the cells are utilizing photons (and CO_2 and nutrients)→ growing.

Use backscattering to estimate C_{phyto}.

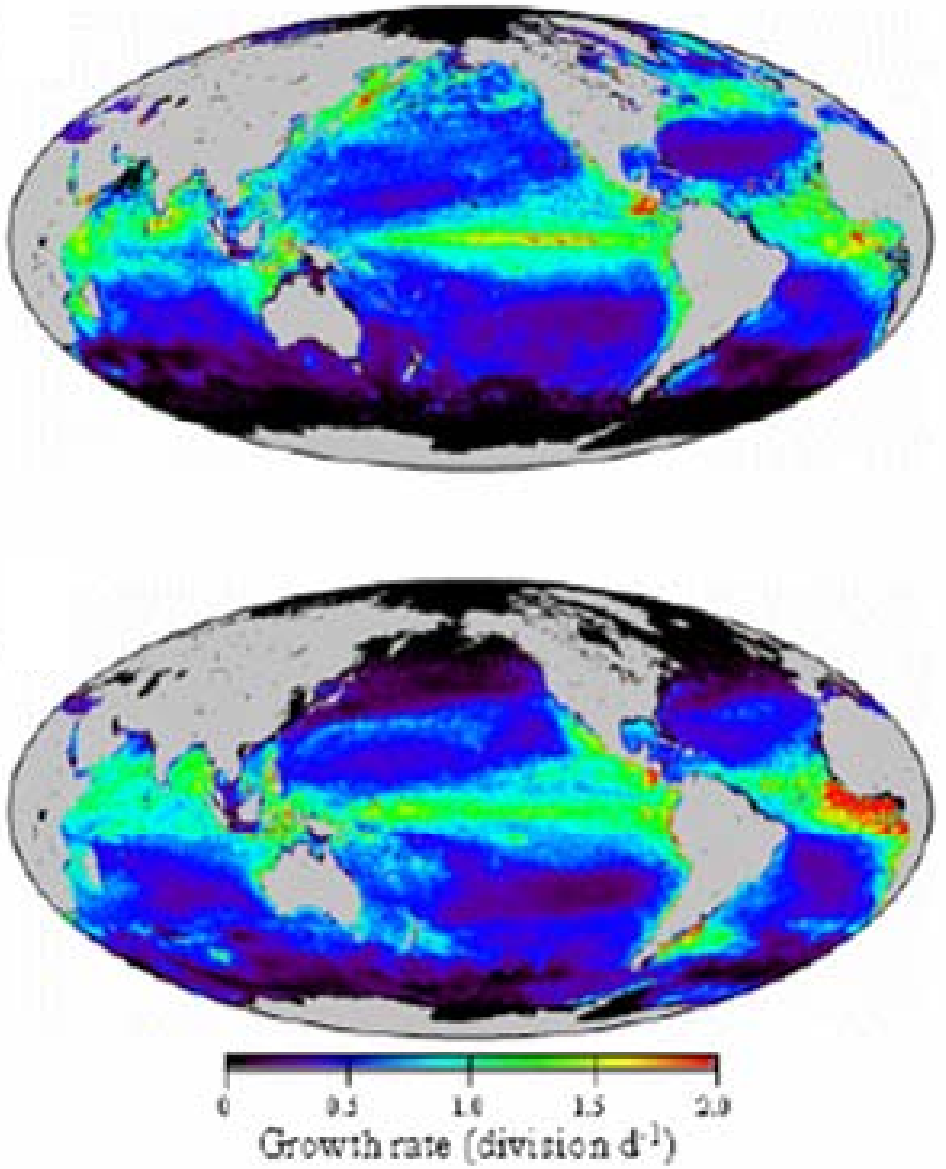

Behrenfeld et al., 2005

Latest: Global fluorescence and quantum yield.

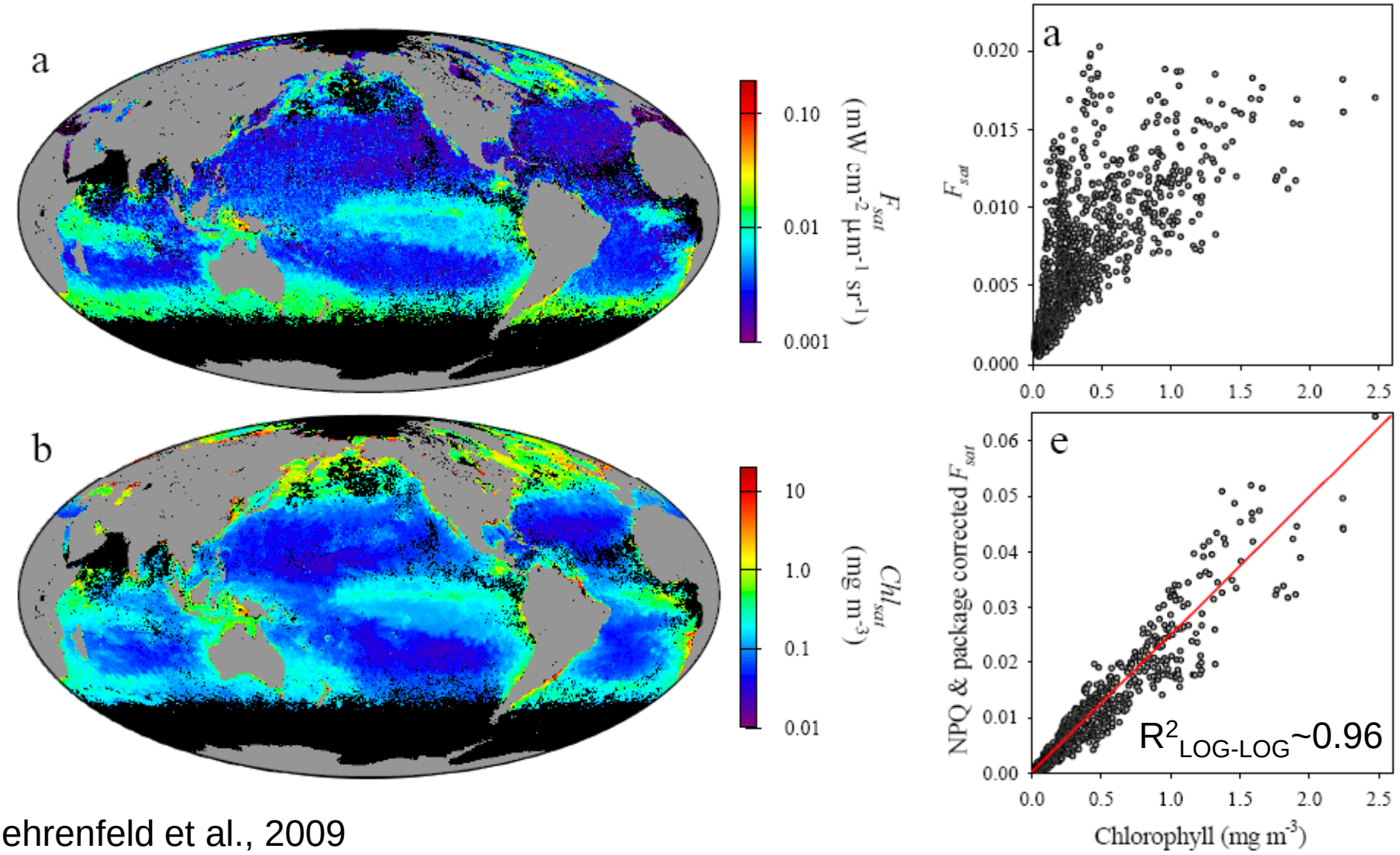

Behrenfeld et al., 2009

φ=F/absorption is an indicator of iron stress

Conclusion

- Reflectance spectra contain a vast amount of information regarding the concentration and composition of particulate and dissolved materials

- Reflectance is theoretically related to the IOPs and empirically related to Chl, thus semi-analytic inversions to IOPs yield lower errors on global scales (without regional tuning) than do chl models

- Much left to do: validation of algorithms, taking advantage of more bands, polarization, LIDAR and more…